Chemical Physics 423 (2013) 85–91

Contents lists available at SciVerse ScienceDirect

Chemical Physics

journal homepage: www.elsevier.com/locate/chemphys

On the use of crystal vibrational modes in the estimation of the anisotropic displacement parameters of hydrogen atoms in molecular crystals: *para*-Nitroaniline as a test case

C. Gustavo Pozzi [a], Adolfo C. Fantoni [a,*], Andrés E. Goeta [b,1], Etelvina de Matos Gomes [d], Garry J. McIntyre [c,2], Graciela Punte [a]

[a] IFLP (CCT-La Plata), Departamento de Física, Facultad de Ciencias Exactas, UNLP CC 67, 1900 La Plata, Argentina
[b] Durham University, Department of Chemistry, South Road, Durham DH1 3LE, UK
[c] Institut Laue-Langevin, 6 Rue Jules Horowitz, BP 156, 38042 Grenoble, France
[d] Center of Physics, University of Minho, Campus de Gualtar, 4710-057 Braga, Portugal

ARTICLE INFO

Article history:
Received 21 March 2013
In final form 3 July 2013
Available online 11 July 2013

Keywords:
Anisotropic displacement parameters
Periodic calculation
Molecular crystal

ABSTRACT

The use of crystal vibrational modes and frequencies calculated for the periodic system to complement a Translation Libration Screw (TLS) fit in the estimation of anisotropic displacement parameters (ADPs) of hydrogen atoms in molecular crystals is proposed. As a test case we have used the *para*-nitroaniline crystal, for which a reference set of ADPs has been obtained by performing a single crystal neutron diffraction study at 100 K. Although the largest difference between estimated and experimental reference values amounts to 0.06 Å^2, this value being about six times the experimental uncertainty, the agreement is better than three experimental uncertainties for 33 out of the total of 36 ADPs. The performance of the suggested method, particularly for the amino atoms, is thoroughly analyzed.

1. Introduction

Organic molecules containing donor and acceptor groups linked through a π-electron system have long been of interest to researchers and materials developers for their applications within the areas of electronics and photonics [1]. *para*-Nitroaniline (pNA) is a prototype for charge-transfer molecules. It has served as an important test system for experimental and theoretical investigations of molecular properties and is a recurrent source for new studies (see for example Ref. [2]).

The interpretation of many of these studies relies on the correct assignment of the molecule's fundamental state. To the best of our knowledge, charge density studies provide the most direct way to obtain detailed quantitative information on the electron density of molecular crystals from experimental data. In such studies, a multipole model is fitted against high resolution X-ray diffraction data [3]. While detailed charge density studies at 100 K have been published for meta-nitroniline (mNA) [4], 2-methyl-4-nitroaniline (2M4NA) [5], and 2-methyl-5-nitroaniline (2M5NA) [6], only fragmentary information from a study at 20 K can be found in the literature for pNA [7]. With the aim of improving the knowledge of molecular aggregation and the sources of the centric or non-centric character of the aggregates we are interested in charge density analysis at 100 K of a series as extended as possible of primary nitroanilines. The atom-centered nature of the involved multipole formalism makes necessary an adequate deconvolution from nuclear motions, whose effect enters the model through the mean square displacement parameters. While anisotropic displacement parameters (ADPs) can reliably be fitted for heavy atoms, hydrogen atoms pose a challenge due to the lack of information about them in the X-ray diffraction data.

Although neutron diffraction is by far the preferred source of H-atoms ADPs, less expensive alternatives to obtain adequate estimations for these parameters have been contemplated. In a recent paper [8], different estimation methods are reviewed and some improvements are proposed. In the present study both approaches have been used for the *para*-nitroaniline crystal. Experimental values have been obtained by performing a single crystal neutron diffraction study at 100 K. The estimation has been undertaken by using a method in which, for the first time,[3] crystal vibrational modes and frequencies are used in conjunction with TLS fit of X-ray data. Using the neutron diffraction results as a reference, the

* Corresponding author. Tel.: +54 221 424 6062; fax: +54 221 425 2006.
E-mail address: fantoni@fisica.unlp.edu.ar (A.C. Fantoni).
[1] Deceased (1965–2011).
[2] Present address: Australian Nuclear Science and Technology Organisation, Lucas Heights NSW 2234, Australia.

[3] One of the reviewers call our attention on a recent paper where a full periodic approach is reported by Madsen et al. [16], but our manuscript was already under revision by the time the reference paper was published.

0301-0104/$ - see front matter © 2013 Elsevier B.V. All rights reserved.
http://dx.doi.org/10.1016/j.chemphys.2013.07.004

conclusions of an exhaustive analysis of the performance of the suggested method, particularly as regards the amino hydrogen atoms, are presented. The pros and cons with respect to other available methods are discussed.

2. Experimental

pNA purchased from a commercial source (Sigma Aldrich) was crystallized by evaporation of a solution in methanol at room temperature. A single crystal with well defined faces and approximate dimensions $1 \times 2 \times 3\ mm^3$ was used to collect monochromatic neutron diffraction data at 100 K. The crystal was mounted on a Displex cryorefrigerator on the ILL thermal-beam diffractometer D19 [9]. Four data sets in the ranges 5°–13°, 3°–29°, 6°–46° and 23°–63° in θ were recorded. Each set corresponds to one of the single microstrip and three multiwire flat square position-sensitive ^{3}He detectors which subtend 15.3° and 20.4°, respectively, at the sample. Data reduction was carried out using the Retreat [10] and Rafd19 programs [11]. Neutron attenuation by the crystal and the cryorefrigerator vacuum and heat shields was corrected by Gaussian integration [12] using the programs D19abs and Abscan based on the Cambridge Crystallography Subroutine Library [13]. With the coordinates from the X-ray structure determination of Tonogaki et al. [14] as a starting point, atomic coordinates and anisotropic displacement parameters for all atoms were refined against F^2 for all data, using SHELXL97 software [15], together with four scale factors and the extinction parameter of the model implemented in SHELXL97. The recommended weighting scheme was used; refined parameters do not change within 3 esd if statistical weights are used instead, in which case the goodness of fit is 2.07 (see Table 1).

Crystal data, detailed information on the diffraction experiment, data reduction and structure refinement are collected in Table 1. The experimental molecular conformation and atom labels are shown in Fig. 1.

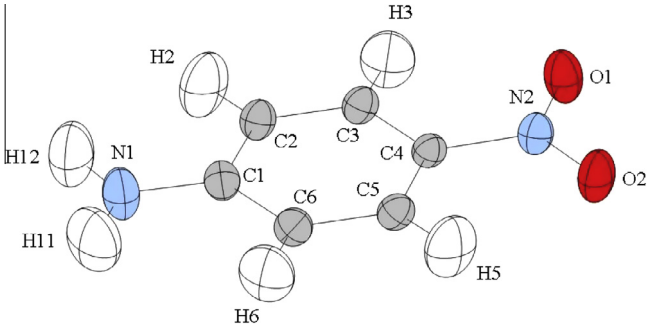

Fig. 1. 75% probability ellipsoid representation of the pNA molecule from neutron diffraction data. Atom numbering scheme is also shown.

Table 1
Experimental Details of the neutron diffraction study.

Crystal data	
Chemical formula	$C_6H_6N_2O_2$
Chemical formula weight	138
Cell setting	Monoclinic
Space group	$P2_1/n$
a, *b*, *c* (Å), β (°)	8.4774(2) 6.0490(1) 12.1040(3) 92.892(1)
V (Å^3)	619.90(2)
Z	4
Radiation type	Neutron
Wavelength (Å)	0.95633 (8)
Absorption coeff. μ (mm^{-1})	0.1520
Temperature (K)	100
Crystal form	Irregular prism
Crystal size (mm)	$3 \times 2 \times 1$
Crystal color	Orange
Data collection	
Radiation source	ILL
Diffractometer	D19
N° of observations	7877
N° of observations, $I > 2\sigma_I$	6011
N° of unique reflections	3633
R_{int}, R_{sigma} (%)	3.5, 4.8
θ_{max}	63°
Range of *h*, *k*, *l*	$-6 \leqslant h \leqslant 15$, $-10 \leqslant k \leqslant 1$, $-22 \leqslant l \leqslant 20$
Absorption correction	Analytic
T_{min}, T_{max}	0.751, 0.880
Structure refinement	
Refinement on	$F^2 > 2\sigma(F^2)$
Weighting scheme	$1/[\sigma(F_o^2)^2 + (0.0232 \cdot P)^2 + 6.37 \cdot P]$
Where $P = (\max$ $(F_o^2, 0) + 2 \cdot F_c^2)/3$	
N_{param}	149
$R[F^2 > 2\sigma(F^2)]$, R[all data], $wR(F^2)$ (%)	4.8, 7.1, 11.4
Goodness of Fit *S*	1.10
Extinction model	Empirical[a]
Extinction coefficient (rad^{-1})	0.0112 (2)
Source of neutron scattering lengths	Int. Tables for crystallography (2006) Vol. C, Table 4.4.4.1

[a] The calculated structure factor F_C is multiplied by $[1 + 0.001xF_C^2\sigma 3/\sin(2\theta)]^{-1/4}$, where *x* is the refined parameter.

3. Calculations

Periodic calculations (PC) were performed with CRYSTAL09 program [17] using the B3LYP hybrid method with the 6-31G** basis set. Shrinking factors equal to 4 were used for both, the Pack–Monkhorst and Gilat nets. Default criteria were used as regards accuracy and SCF convergence. Atomic positions were optimized keeping the cell parameters at their experimental values (see Table 1). Default optimization criteria were also used in this case. Vibrational frequencies at the Γ point [18] were then calculated for the optimized geometry.

Calculations on the isolated molecule were performed with Gaussian 03 [19], using the B3LYP hybrid method with the 6-31G** basis set and default convergence criteria for SCF and geometry optimization.

The choice of the level of theory, in particular for periodic calculations, deserves some specific considerations. Taking as a reference molecular geometry optimizations at different levels, it can be concluded that pyramidality of the amino group is sensibly larger in the isolated pNa molecule than in its experimental crystal counterpart. On this basis, the good agreement with experiment of the geometry of the amino group in the crystal optimized geometry can be taken as an indicator of the goodness of the B3LYP/6-31G** level of theory to account not only for the intermolecular interactions but also, and more important, for the crystal field. On the basis of molecular calculations we have in fact verified that in the single molecule the degree of pyramidalization of the amino group can be controlled by applying suitable uniform electric fields of the same order of magnitude of the mean crystal one. On the other hand, only little changes in the amino group geometry are observed when the empirical GRIMME correction [20] is included, a fact that would rule out any significant influence of dispersive interactions. It is also worth mentioning that the inclusion of cell parameters in the optimization – either with or without GRIMME correction – does not lead to significant changes in the amino group geometry, though only in the first case a reasonable agreement with experimental values of the cell parameters can be obtained by using a suitable scale factor.

3.1. Estimation of the ADPs of hydrogen atoms

In most methods to estimate H atom ADPs that rely on information extracted from a theoretical model to supplement X ray diffraction data, the ADP for atom H_n is obtained as the sum of two terms:

$$U_{ij}(H_n) \equiv U_{ij}(H_n; \mathrm{TLS(exp)}) + \Delta U_{ij}(H_n; \mathrm{model}) \quad (1)$$

The first term is the result of the extrapolation of a TLS model [21] (possibly a segmented one) fit to the experimentally determined heavy atom ADPs. The TLS model describes the mean squared displacements of a set of nuclei under the assumption that they are part of a rigid body. This is done by means of three tensors, the components of which (twenty independent parameters altogether) can be linearly fit to the nuclear ADPs once the equilibrium coordinates are known. The second term, which can conveniently referred to as an estimation of the residual H_n atom ADP [22] is calculated from the normal modes of a theoretical model.

Methods differ among themselves in the model employed, but also in the way vibrational information is taken into account in the estimation of the residual ADPs. In the present work a periodic model is used and residual ADPs are estimated as

$$\Delta U_{ij}(H_n; \mathrm{model}) \equiv U_{ij}(H_n; \mathrm{model}) - U_{ij}(H_n; \mathrm{TLS(model)}) \quad (2)$$

Although probably not evident at first sight, the procedure outlined above should be equivalent to the so called TLS + ONIOM method [23]. As pointed out in the introduction, however, improvement with respect to that proposal could in principle be expected if vibrational information obtained from periodic calculations was used. We will borrow that acronym and refer to the present implementation as TLS + CRY.

Using the program CRYSTAL09 [17] it is possible, in principle, to characterize the complete set of normal modes (phonons) of a periodic model system. That means the calculation of the eigenvalues $\Omega_k(\boldsymbol{q})$ and eigenvectors $\theta_k(\boldsymbol{q})$ of the dynamical matrix $\mathbf{D}(\boldsymbol{q})$ for a set, as complete as wished, of N_C values of the wavevector $\boldsymbol{q}$ in the reciprocal unit cell. With that information at hand, the model ADPs for the model crystal in statistical equilibrium at the temperature T would be obtained as

$$U^C_{ij}(n) = \frac{1}{N_C}\sum_q\sum_k U^C_{ij}(n; k\boldsymbol{q}) \quad (3)$$

where

$$U^C_{ij}(n; k\boldsymbol{q}) = (\hbar/2m_n\Omega_k(\boldsymbol{q}))coth(\hbar\Omega_k(\boldsymbol{q})/2T)\theta_i(n; k\boldsymbol{q})\theta^*_j(n; k\boldsymbol{q}) \quad (4)$$

Due to the high computational cost of such a kind of calculation – which implies the reduction of the symmetry by means of the use of a supercell–, its use as part of a method for estimating H atom ADPs can hardly be justified. But even if only results obtained for the Γ point were used, some non minor advantages with respect to the ONIOM approach are to be expected. On the one hand, the exploitation of the full crystal symmetry allows intermolecular interactions to be much more realistically taken into account at a reasonable computational expense. Moreover, results will be free from any effect concerning the conditional convergence of the electric field inside a polar medium as a function of the cluster size and shape. On the other hand, the restriction of a rigid environment for the sample molecule is relaxed, a fact that should be expected to lead to an improvement in the description of the correlation between the intramolecular (internal) distortions and the overall (external) molecular motion.

In this no-dispersion approximation, model ADPs are computed solely from the $\boldsymbol{q} = 0$ phonons. Formally, the dependence of $\mathbf{D}$ on $\boldsymbol{q}$ is neglected, and as a consequence $\Omega_k(\boldsymbol{q}) \equiv \Omega_k(\mathbf{0})$ and $\Theta(\boldsymbol{q}) \equiv \Theta(\mathbf{0})$. This approximation is expected to be a reasonable one for the highest frequency bands in molecular crystals, but in this context it is clearly invalid for the acoustic ones, for which Ω_k is exactly zero at $\boldsymbol{q} = 0$. Since the contribution of mode $k\boldsymbol{q}$ to $U^C(n)$ (Eq. (5)) diverges as $\Omega_k(\boldsymbol{q})^{-2}$ when $\Omega_k(\boldsymbol{q})$ approaches zero (Eq. (5)), acoustic branches must be entirely excluded in this approach. Under these circumstances, with $k = 1,2,3$ labeling the acoustic branches, Eq. (3) becomes:

$$U^C_{ij}(n; \mathrm{model}) = \sum_{k>3} U^C_{ij}(n; k\mathbf{0}) \quad (5)$$

4. Results and discussion

4.1. para-Nitroaniline neutron diffraction

Bond lengths obtained from neutron diffraction data and from geometry optimizations performed on the crystal and on the isolated molecule are collected in Table 2. Experimental and optimized atomic coordinates, intramolecular bond angles, torsion angles and atomic distances from the six-membered aromatic can be found in the supplementary material.

The crystal structure of *p*NA (monoclinic $P2_1/n$) has been described by Panunto et al. [24] in terms of polar chains generated by an N–H···O hydrogen bond (N1–H12···O1^i, see Table 6) that connects molecules related by a glide operation. Chains are arranged into polar layers by a second, longer and less directional N–H···O interaction (N1–H11···O2^{ii}), and layers are packed centrosymmetrically. This description is not altered in its main features in the light of the present results.

As regards the neutron diffraction values, the most interesting result is the difference between the two N–O bond lengths (0.009 Å), the N2–O1 being the largest. This fact is consistent with

Table 2
pNA Bond lengths (Å). Standard deviations in parenthesis.

		Experimental	optmized	
			Crystal	Monomer
O1	N2	1.245(1)	1.252	1.234
O2	N2	1.236(1)	1.243	
N1	C1	1.359(1)	1.349	1.394
N2	C4	1.436(1)	1.421	1.463
C1	C2	1.417(1)	1.423	1.405
C1	C6	1.417(1)	1.423	
C2	C3	1.382(1)	1.375	1.389
C5	C6	1.383(1)	1.379	
C3	C4	1.401(1)	1.408	1.392
C4	C5	1.401(1)	1.407	
N1	H11	0.994(2)	1.010	1.009
N1	H12	1.011(2)	1.012	
C2	H2	1.083(2)	1.083	1.084
C6	H6	1.084(2)	1.083	
C3	H3	1.080(2)	1.080	1.080
C5	H5	1.083(2)	1.082	

Table 3
Intermolecular X–H···O contacts from neutron diffraction data. Standard deviations in parenthesis.

		H···O (Å)	X···O (Å)	X–H···O (°)
I	N1–H12···O1^i	2.030(2)	3.038(1)	174.8(2)
II	N1–H11···O2^{ii}	2.247(2)	3.086(1)	141.2(2)
III	C2–H2···O2^i	2.606(2)	3.412(1)	130.7(2)
IV	C3–H3···O1^{iii}	2.384(2)	3.248(1)	136.0(2)
V	C5–H5···O2^{iv}	2.655(2)	3.480(1)	132.6(2)

i: −0.5 + *x*, 1.5 − *y*, 0.5 + *z*; *ii*: −0.5 + *x*, 0.5 − *y*, 0.5 + *z*; *iii*: 1 − *x*, 2 − *y*, −*z*; *iv*: 2 − *x*, 1 − *y*, −*z*.

Table 4
Experimental ADPs (10^{-4} Å^2) (first line) and their TLS + CRY estimations using the N1–6C–N2 fragment for the TLS fit (second line). Standard deviations in parenthesis.

	U11	U22	U33	U12	U13	U23	*S*	*q*
H11	498(11)	272(7)	414(10)	18(8)	100(8)	126(7)		
	469	318	427	35	111	146	0.20	3.3
H12	343(8)	399(9)	345(8)	28(7)	148(6)	48(7)		
	326	403	334	29	131	33	0.06	1.8
H2	300(7)	395(9)	347(8)	108(7)	141(6)	6(7)		
	310	351	364	103	143	18	0.15	2.4
H3	358(8)	227(6)	349(8)	91(6)	60(6)	48(6)		
	345	228	342	83	62	60	0.05	1.2
H5	317(8)	317(7)	368(8)	125(7)	126(6)	5(7)		
	321	300	343	110	109	-4	0.12	2.2
H6	397(9)	209(6)	364(8)	61(6)	47(6)	70(6)		
	393	226	370	69	49	78	0.04	1.4

the relation between the N1–H12···O1 and N1–H11···O2 hydrogen bonds, the former being shorter and more directional. It is worth noting that internal coordinates obtained from the crystal geometry optimization lead to the same conclusions. Experimental N2–O2 and N2–O1 bond lengths are both 0.007 Å shorter than their counterparts in the crystal optimized geometry, differences very well accounted for by the riding model corrections. The neutron diffraction N2–O2 bond length is very similar to its isolated molecule value, but there is a difference of 0.011 Å as regards N2–O1, the experimental value being the largest. Experimental values of the C–N bond lengths are underestimated in the crystal geometry optimization (0.010 Å and 0.015 Å for N1–C1 and N2–C4, respectively), while values obtained for the isolated molecule are larger than the experimental ones (0.035 Å and 0.027 Å, for N1–C1 and N2–C4, respectively). The differences in C–C bond lengths between the three data sets are consistent with those described for the C–N ones, since C1–C2 and C1–C6 decrease 0.018 Å and C2–C3 and C6–C5 increase 0.012 Å on the average, in going from the isolated molecule to the optimized crystal structure, the experimental values being approximately midway. It would seem that crystallization leads to a somewhat more quinonoidal molecular geometry, an effect that appears overestimated by the periodic geometry optimization.

Table 6
Experimental (exp) and theoretical (cry) mean values of the diagonal residual MSDT components (10^{-4} Å^2) of the aromatic hydrogens in the local axial systems (first and third lines) and the maximum deviations from those means (second and fourth lines).

	6C–N2			N1–6C–N2			N1–6C		
	ΔU_{AA}	ΔU_{BB}	ΔU_{CC}	ΔU_{AA}	ΔU_{BB}	ΔU_{CC}	ΔU_{AA}	ΔU_{BB}	ΔU_{CC}
exp	44	157	218	43	159	185	42	166	147
	9	16	31	9	17	46	10	19	33
cry	49	146	207	49	144	180	49	140	150
	1	5	18	1	6	16	1	6	18

The deviation of the molecule from a planar structure agrees with the Trueblood et al. [25] and Tonogaki et al. reports [14].

The almost planar and slightly twisted geometry of the C–NH_2 moiety is confirmed by the present results. Indeed, the N1–C1 bond departs 1.9(2)° from the N–H_2 plane, the average acute torsion C–C–N–H angle being 5.5(2)°. Values for these angles are reproduced within 1° by the periodic optimization. The twisting direction of the amino group is clearly determined by the location of the acceptor O atoms of the hydrogen bonds (see Table 3).

4.2. ADPs of hydrogen atoms estimated with the TLS + CRY approach

ADPs of the hydrogen atoms estimated using the six carbon atoms and two nitrogen atoms as the molecular fragment for the TLS fit [26] (N1–6C–N2 fragment) are collected in Table 4, together with the experimental values. For each atom, the percentage value of the similarity index S_{12} introduced by Whitten and Spackman [23] provides an overall comparison of estimated and experimental mean squared displacement tensors (MSDT). The weighted root mean square difference over the six independent ADPs

Table 5
Experimental (exp) and theoretical (cry) residual H atoms ADPs (10^{-4} Å^2) according to the TLS models fit to the fragments 6C–N2, N1–6C–N2 and N1–6C, each expressed in a local system of axes defined for each atom (see Fig. 3).

		H11						H12					
		ΔU_{AA}	ΔU_{BB}	ΔU_{CC}	ΔU_{BC}	ΔU_{CA}	ΔU_{AB}	ΔU_{AA}	ΔU_{BB}	ΔU_{CC}	ΔU_{BC}	ΔU_{CA}	ΔU_{AB}
6C–N2	exp	16	169	312	26	−38	−3	52	113	221	28	−14	−5
	cry	47	159	309	−8	−1	−5	52	135	167	18	−5	−10
N1–6C–N2	exp	19	172	192	24	−27	−7	55	116	101	18	−7	−9
	cry	44	156	212	−3	4	−2	48	132	71	12	−7	−7
N1–6C	exp	21	177	147	22	−26	−11	58	119	63	13	−6	−13
	cry	42	153	178	0	4	0	47	130	40	9	−8	−5
SHADE2[a]		51	138	200	0	0	0	51	138	200	0	0	0
		H2						H6					
		ΔU_{AA}	ΔU_{BB}	ΔU_{CC}	ΔU_{BC}	ΔU_{CA}	ΔU_{AB}	ΔU_{AA}	ΔU_{BB}	ΔU_{CC}	ΔU_{BC}	ΔU_{CA}	ΔU_{AB}
6C–N2	exp	43	169	224	−10	−4	−14	42	141	199	6	−12	0
	cry	49	142	225	4	−1	0	48	144	203	−1	2	0
N1–6C–N2	exp	42	171	175	−16	−2	−14	41	142	152	1	−10	−1
	cry	49	138	184	2	−1	1	48	142	164	−3	3	1
N1–6C	exp	41	175	155	−19	−7	−12	40	147	127	0	−15	1
	cry	49	135	168	0	−3	0	48	139	146	−2	3	0
SHADE2[a]		47	146	232	0	0	0	47	146	232	0	0	0
		H3						H5					
		ΔU_{AA}	ΔU_{BB}	ΔU_{CC}	ΔU_{BC}	ΔU_{CA}	ΔU_{AB}	ΔU_{AA}	ΔU_{BB}	ΔU_{CC}	ΔU_{BC}	ΔU_{CA}	ΔU_{AB}
6C–N2	exp	53	157	199	−16	−2	−5	37	162	249	−3	8	1
	cry	48	148	191	−6	1	2	49	151	210	−1	−3	1
N1–6C–N2	exp	52	158	181	−14	−5	−6	36	163	231	−2	4	0
	cry	49	145	177	−4	0	4	49	150	194	−2	−5	1
N1–6C	exp	52	167	125	−5	−2	−4	35	174	180	4	6	3
	cry	49	140	135	−2	0	2	50	146	152	0	−3	0
SHADE2[a]		47	146	232	0	0	0	47	146	232	0	0	0

[a] From Ref. [8].

Table 7
N1 residual ADPs (10^{-4} Å^2) after the TLS fit to the 6C–N2 fragment.[a]

	ΔU_{AA}	ΔU_{BB}	ΔU_{CC}	ΔU_{AB}	ΔU_{CA}	ΔU_{BC}
Isolatedmonomer	2	15	77	0	−2	0
ONIOM4Å	−1	1	94	3	−3	−3
ONIOM6Å	−1	1	237	5	1	4
ONIOM8Å	−1	2	444	4	3	16
Periodicmodel	0	7	75	1	4	9
Experimental	6	−4	92	0	1	19

[a] Expressed in a local Cartesian system: *A* axis parallel to N1–C1, *C* axis perpendicular to the N1 C1 C6 plane.

$$q(H) = \left[\frac{1}{6}\sum_{i<j}\left(\frac{U_{ij}^{EXP}(H) - U_{ij}^{EST}(H)}{\sigma_{ij}^{EXP}(H)}\right)^2\right]^{\frac{1}{2}}$$

is also included in Table 4. In the expression above $\sigma_{ij}^{EXP}(H)$ is the experimental estimated uncertainty (standard deviation) of $U_{ij}^{EXP}(H)$. THMA14 [27] as implemented in the WinGX [28] package of crystallographic programs was used for the TLS fits.

Out of the 36 individual ADPs, 33 are reproduced within three times the experimental uncertainty, 22 of them being within twice the uncertainty. The most poorly predicted parameters are U_{22}(H11), which is overestimated by 46×10^{-4} Å^2 (six and a half times the uncertainty), and U_{22}(H2) and U_{33}(H5), which are underestimated by 44×10^{-4} Å^2 (about four times the uncertainty) and 25×10^{-4} Å^2 (three times the uncertainty), respectively.

The comparison between an estimated MSDT and its experimental (reference) counterpart can also be performed in terms of the eigenvalues and eigenvectors of their difference when expressed in a cartesian axial system. Given a unitary vector whose cartesian components are arranged in the column matrix $\boldsymbol{n}$, and the square matrix $\boldsymbol{U}$ that represents an atomic MSDT in that axial system, the quantity $\xi^2(\boldsymbol{n}) = \boldsymbol{n}^t\boldsymbol{U}\boldsymbol{n}$ represents the atomic mean square displacement amplitude (MSDA) along $\boldsymbol{n}$. Therefore, the eigenvectors of the difference U_1 - U_2 indicate the directions for which thedifference $\Delta\xi^2(\boldsymbol{n}) = \xi_1^2(\boldsymbol{n}) - \xi_2^2(\boldsymbol{n})$ between MSDAs is stationary with respect to the direction $\boldsymbol{n}$. In particular, the eigenvector of $\boldsymbol{U}^{EST} - \boldsymbol{U}^{EXP}$ corresponding to the largest magnitude eigenvalue shows the direction in which the predicted MSDA differs most from the reference one. Eigenvectors for the H atoms are schematically represented in Fig. 2, where eigenvalues are also included. In the case of H2 the largest magnitude eigenvalue (-47×10^{-4} Å^2) is found in a direction forming 72° with the C2–H2 bond and 19° with the ring mean plane (underestimation of the in-plane bending amplitude). For H5 themaximum discrepancy in MSDAs amounts to -41×10^{-4} Å^2 and occurs in a direction forming 77° with the C5–H5 bond and 77° with the ring plane (underestimation of the out-of-plane bending amplitude).

It is to be noted that according to both experimental and theoretical data the atomic ADPs within the N1–6C–N2 fragment are not satisfactorily described by the TLS model. The individual residuals ΔU_{ij} for the involved atoms are consistent with the effect of an additional out-of-plane or inversion motion of N1 relative to the 6C–N2 skeleton. This is more clearly evidenced in the residual MSDT of N1 after the TLS fit to the 6C–N2 fragment (see Table 4), which has a component of 92×10^{-4} Å^2 in the direction normal to the molecular mean plane according to the experimental data, and 75×10^{-4} Å^2 according to the theoretical model. It should be remarked that if the residual ADPs ΔU_{ij}(N1) after the TLS fit to 6C–N2 were equal in the theoretical and the experimental data, then the estimated ADPs for the H atoms would be the same whether N1 is included in the fragment or not, irrespective of the magnitude of ΔU_{ij}(N1). Taking into account that this is not exactly the case here, H atoms ADPs were also estimated using two other fragments for the TLS fit: the six carbons and the amino nitrogen (N1–6C), and the six carbons and the nitro nitrogen (6C–N2). Individual U_{ij} values differ from those in Table 4 at most in 14×10^{-4} Å^2, amounting to 2.5 times the uncertainty in the corresponding experimental value. No overall improvement is obtained. In fact, with the 6C–N2 fragment, the agreement between estimated and experimental ADPs worsens for the amino hydrogen

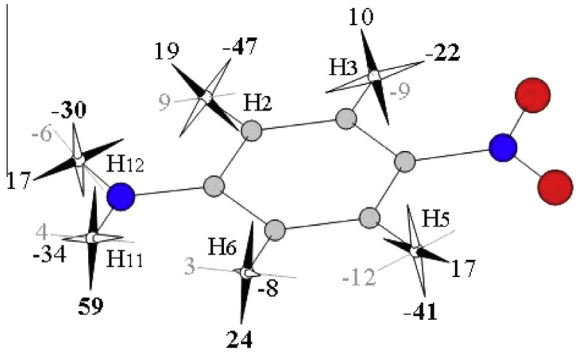

Fig. 2. Eigenvectors and eigenvalues (10^{-4} Å^2) of the differences $\boldsymbol{U}^{EST} - \boldsymbol{U}^{EXP}$ corresponding to the data in Table 1. Solid and empty spikes and thin lines indicate the eigenvectors corresponding to the maximum, minimum and medium eigenvalues, respectively.

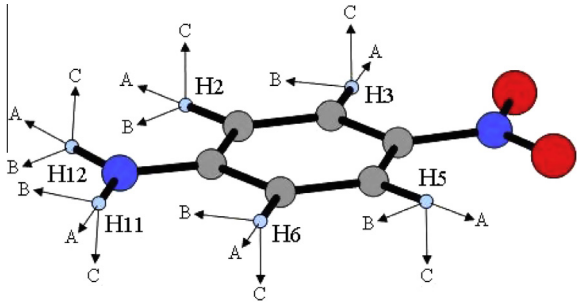

Fig. 3. Cartesian local axial systems defined for the hydrogen atoms: bond directed (A), in-plane (B) and out-of-plane (C) axes.

Table 8
Electric field values in the 4 Å and 8 Å models (10^{-3} a.u.). Components in the inertial axial system of the N1–6C–N2 fragment.

	ONIOM4 Å				ONIOM8 Å			
	E_1	E_2	E_3	$\|E\|$	E_1	E_2	E_3	$\|E\|$
C1	9.91	−3.32	1.25	10.53	7.06	−0.77	−1.93	7.36
N1	11.06	−2.97	2.58	11.74	8.96	−0.04	−1.08	9.02
H11	15.93	−2.61	0.80	16.16	14.10	0.48	−1.29	14.17
H12	8.63	−7.76	4.57	12.47	6.70	−4.01	1.90	8.04
Mean	11.01	−2.73	0.72	11.37	8.29	−0.49	−1.52	8.45
Standard deviation	3.40	4.09	2.60		3.36	3.80	2.61	

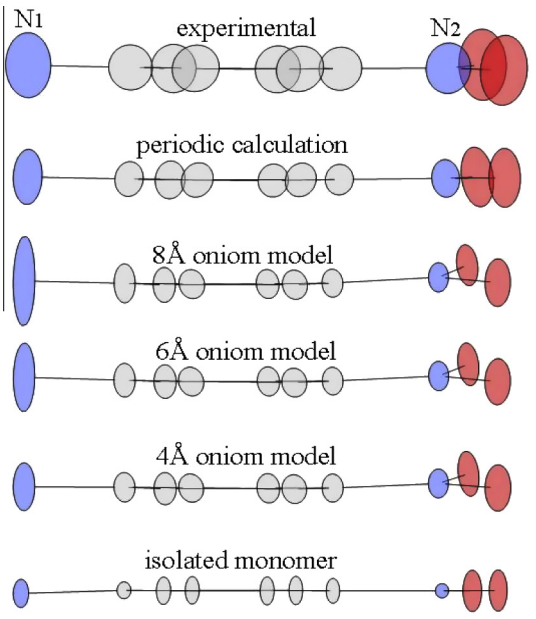

Fig. 4. Ellipsoid representation (90% probability) of the heavy atoms MSDT.

atoms and slightly improves for the aromatic ones, and the converse applies when N1–6C is used. In any case, the U_{22} components of H2 and H11 remain poorly reproduced.

In contrast to the marginal sensitivity of the estimated ADPs to the choice of the TLS fragment, the H atom residual ADPs show a strong dependence, particularly those of the amino hydrogen atoms. The experimental and theoretical values of the residual MSDT components expressed in a local system of axes defined individually for each atom (see Fig. 3) are gathered in Table 5, together with the values used by the SHADE2 web server [8] for estimation of the ADPs of hydrogen atoms. The experimental values of the out-of-plane components ΔU_{CC} of H11 and H12 experience a reduction of 120×10^{-4} Å^2 when N1 is added to R–N2, and about 40×10^{-4} Å^2 when N2 is excluded from N1–6C–N2. The remaining components are less sensitive to the choice of the fragment. In the case of the theoretical data, the smaller out-of-plane residual component of N1 after the TLS fit to 6C–N2 leads to a less pronounced dependence of ΔU_{CC} with the choice of the TLS fragment, with reductions of 95×10^{-4} Å^2 and 30×10^{-4} Å^2 in the sequence 6C–N2 → N1–6C–N2 → N1–6C. Regarding the aromatic hydrogen atoms, the residual out-of-plane components are reduced by about 70×10^4 Å^2 in the experimental model and 60×10^{-4} Å^2 in the theoretical one when going from 6C–N2 to N1-6C, those of H2 and H6 being more sensitive to the inclusion of N1 in the TLS fragment than to the removal of N2, and conversely for H3 and H5.

Interestingly, the residual ADPs of the two amino hydrogen atoms are found not to be equal. Regardless of the fragment chosen for the TLS fit, the experimental values for ΔU_{BB} and ΔU_{CC} of H12 are, respectively, about 55×10^{-4} Å^2 and 90×10^{-4} Å^2 smaller than those of H11. Although the estimation of uncertainties for these values is not straightforward, those differences are probably significant, particularly the latter. They are qualitatively reproduced by the theoretical model, the difference between in-plane components being about 25×10^{-4} Å^2, smaller than the experimental one, and that between out-of-plane components about 140×10^{-4} Å^2, even larger than its experimental counterpart. Regarding the aromatic hydrogen atoms the mean values of the diagonal residual components are in reasonable agreement with the values used by the SHADE2 web server [8] when the 6C–N2 fragment is used (see Table 6).

It is tempting to associate the small value of ΔU_{CC}(H12) compared to ΔU_{CC}(H11) with the fact that in this structure H12 is involved in a shorter and more directional H bond than H11 is. This interpretation seems to be supported by the theoretical model, since ΔU_{CC}(H12) is smaller than its experimental counterpart by 30×10^{-4} Å^2, and the H12···O2 contact is shorter (1.925 Å vs. 2.030(2) Å).

Two issues can be remarked. In the first place, the observed difference between the residual MSDT of the amino hydrogen atoms raises a warning against the use of an only set of ADPs for each chemical type of hydrogen, since individuals within a given type are usually in different environments in the crystal. It should be mentioned that the statistical frequency of this situation in molecular crystals is surely at the origin of the large rms deviations of the amino hydrogen atom parameters in SHADE2 data base. Both experimental and theoretical values for ΔU_{CC}(H11) would be closely reproduced by the SHADE2 web server [8] if the N1–6C–N2 fragment was used, but in that case ΔU_{CC}(H12) would be severely overestimated. Moreover, the situation would be even worse if the minimal N1–6C fragment was used, and this fact concerns the second issue we would like to address here: the internal motion of the amino nitrogen relative to the rest of the molecule.

Our first attempts to estimate the H atoms ADPs in the pNA crystal structure were conducted following the finite, rigid environment method proposed by Whitten and Spackman [23]. The central molecule (high level subsystem in the ONIOM calculation) was modeled at the B3LYP/6-31G**, and its interaction with the environment with the UFF force field supplemented with atomic point charges. Atomic positions were extracted from the experimental model, the environment being defined as the set of molecules with at least one atom···atom distance from the central one shorter than a given threshold D. Environments of three sizes were tested, given by $D = 4$ Å (13 molecules), 6 Å (26 molecules) and 8 Å (44 molecules). Atomic charges were adjusted so that they best reproduce the values of the electric field at a grid of points uniformly chosen on the Hirshfeld surface of the reference molecule in the periodic model.

The MSDT of the amino nitrogen was found to depend strongly on the size of the environment, as evidenced by the ellipsoid representations in Fig. 4. As shown in Table 7, the N1 out-of-plane residual diagonal component in the 4 Å model matches the experimental one, but, rather unexpectedly, it grows dramatically as the size of the environment is increased. Data for the isolated B3LYP/6-31G** monomer are also included in the table, which shows that the out-of-plane N1 residual MSDA with respect to the 6C–N2 fragment is already appreciable in that model.

Since the UFF part of the external potential decays as r^{-6}, the sensitivity of the amino nitrogen ADPs to the details of the model is most likely related to differences in the electrostatic potential experienced by the central molecule in the three models. The values of the electric field components at the atomic positions of the C–NH_2 group, as well as the mean values over the sixteen atomic positions and the corresponding standard deviations in the 4 Å and 8 Å models are reported in Table 8. The difference between the electric field in the 8 Å model and the 4 Å model one is almost uniform over the atomic positions.

5. Conclusions

In the present paper, accurate positions and ADPs of hydrogen atoms in the title compound determined from a neutron diffraction study at 100 K are reported, as well as estimated values of the ADPs resulting from a method (TLS + CRY) relying on a TLS fit and a vibrational frequency calculation on the periodic system. We have shown that in approaches of this kind an appropriate description of

the electrostatic field acting on each molecule can be crucial for the correct modeling of the amino vibrational properties. Despite the present system being non polar, if a finite cluster of molecules is used the resulting electrostatic field depends on the cluster size. For polar systems, where the electric field calculated at points inside the crystal is only conditionally convergent as a series over the contributions of the individual molecules, using finite clusters of molecules, however large they are built, the resulting electric field would lack any credibility. In this respect, assuming the electric field at positions inside a real crystal is truly described by the Ewald field (summation for the infinite periodic system), the normal modes obtained from the periodic calculation should automatically overcome the convergence problem, giving much more confidence to the obtained results.

Finally, our results show that the vibrational behavior of amino hydrogen atoms in a crystal may be sufficiently dependent on the intermolecular interactions in which they are individually involved so as to invalidate any attempt to model their ADPs if such dependency is disregarded.

In summary, owing to its very reasonable benefits cost ratio we think that in the lack of neutron diffraction data the estimation method proposed here should become the preferred choice when ADPs are to be used in a charge density study.

Acknowledgements

This work was supported by grants from CONICET (PIP 0985) and UNLP (Project X577). A. C. Fantoni and G. P. are members of CONICET.

References

[1] L.R. Dalton, P.A. Sullivan, D.H. Bale, Chem. Rev. 110 (2010) 25.
[2] Y.C. Chan, K.Y. Wong, J. Chem. Phys. 136 (2012) 174514;
D. Kosenkov, L.V. Slipchenko, J. Phys. Chem. A 115 (2011) 392;
S. Sok, S.Y. Willow, F. Zahariev, M.S. Gordon, J. Phys. Chem. A 115 (2011) 9801;
H. Reis, J. Chem. Phys. 125 (2006) 014506-1.
[3] R.F. Stewart, Isr. J. Chem. 16 (1977) 124;
N.K. Hansen, P. Coppens, Acta Crystallogr. A34 (1978) 909.
[4] C.G. Pozzi, A. Fantoni, G. Punte, A.E. Goeta, Chem. Phys. 358 (2009) 68.
[5] A.E. Whitten, P. Turner, W.T. Klooster, R.O. Piltz, M.A. Spackman, J. Phys. Chem. A 110 (2006) 8763.
[6] J. Ellena, A.E. Goeta, J.A.K. Howard, G. Punte, J. Phys. Chem. A 105 (2001) 8696.
[7] A. Volkov, C. Gatti, Y. Abramov, P. Coppens, Acta Crystallogr. A56 (2000) 252.
[8] P. Munshi, A.Ø. Madsen, M.A. Spackman, S. Larsen, R. Destro, Acta Crystallogr. 64 (2008) 465.
[9] M. Thomas, R.F.D. Stansfield, M. Berneron, A. Filhol, G. Greenwood, J. Jacobe, D. Feltin, S.A. Mason, in: P. Convert, J.B. Forsyth (Eds.), Position-Sensitive Detection of Thermal Neutrons, Academic Press, London, 1983, p. 344.
[10] C. Wilkinson, H.W. Khamis, R.F.D. Stansfield, G.J. McIntyre, J. Appl. Crystallogr. 21 (1988) 471.
[11] A. Filhol, RAFIN, RAFNB, RAFDB, RAFD19: programs for the refinement of the [UB] matrix, wavelength, cell parameters instrument zero shifts in a single crystal diffraction experiment, Technical Report ILL 87FI19T, Institut Max von Laue, Paul Langevin, Grenoble, 1987.
[12] P. Coppens, L. Leiserowitz, D. Rabinovich, Acta Crystallogr. 18 (1965) 1035.
[13] J.C. Matthewman, P. Thompson, P.J. Brown, J. Appl. Crystallogr. 15 (1982) 167.
[14] M. Tonogaki, T. Kawata, S. Ohba, Y. Iwata, I. Shibuya, Acta Crystallogr. B49 (1993) 1031.
[15] G.M. Sheldrick, Acta Crystallogr. A64 (2008) 112.
[16] A.Ø. Madsen, B. Civalleri, M. Ferrabone, F. Pascale, A. Erba, Acta Cryst. A69 (2013) 309.
[17] R. Dovesi, R. Orlando, B. Civalleri, C. Roetti, V.R. Saunders, C.M. Zicovich-Wilson, Z. Kristallogr. 220 (2005) 571;
R. Dovesi, V.R. Saunders, C. Roetti, R. Orlando, C.M. Zicovich-Wilson, F. Pascale, B. Civalleri, K. Doll, N.M. Harrison, I.J. Bush, P. D'arco, M. Llunel, CRYSTAL09 User's Manual, University of Torino, Torino, 2009.
[18] F. Pascale, C.M. Zicovich-Wilson, F. Lopez, B. Civalleri, R. Orlando, R. Dovesi, J. Comput. Chem. 25 (2004) 888;
C.M. Zicovich-Wilson, F. Pascale, C. Roetti, V.R. Saunders, R. Orlando, R. Dovesi, J. Comput. Chem. 25 (2004) 1873.
[19] M.J. Frisch, G.W. Trucks, H.B. Schlegel et al., Gaussian 03, Revision E.01, Gaussian, Inc., Wallingford, CT, 2004.
[20] S. Grimme, J. Comput. Chem. 27 (2006) 1787;
B. Civalleri, C.M. Zicovich-Wilson, L. Valenzano, P. Ugliengo, Cryst. Eng. Commun. 10 (2008) 405;
B. Civalleri, C.M. Zicovich-Wilson, L. Valenzano, P. Ugliengo, Cryst. Eng. Commun. 10 (2008) 1693.
[21] V. Schomaker, K.N. Trueblood, Acta Crystallogr. B24 (1968) 63.
[22] A.Ø. Madsen, S. Mason, S. Larsen, Acta Crystallogr. B59 (2003) 653.
[23] A.E. Whitten, M.A. Spackman, Acta Crystallogr. B62 (2006) 875.
[24] T.W. Panunto, Z. Urbánczyk-Lipkowska, R. Johnson, M.C. Etter, J. Am. Chem. Soc. 109 (1987) 7786.
[25] K.N. Trueblood, E. Goldish, J. Donohue, Acta Crystallogr. 14 (1961) 1009.
[26] J.D. Dunitz, X-ray Analysis the Structure of Organic Molecules, VCH, Weinheim, 1995, pp 244 (Chapter 5); J.D. Dunitz, V. Schomaker, K.N. Trueblood, J. Phys. Chem. 92 (1988) 856; J.D. Dunitz, E.F. Maverick, K.N. Trueblood, Angew. Chem. Int. Ed. Engl. 27 (1988) 880.
[27] K.N. Trueblood, E.F. Maverick, THMA14c for MS-Windows, version of March 11, 1999, University of California, Los Angeles, USA.
[28] L.J. Farrugia, J. Appl. Cryst. 32 (1999) 837.